

FIRST INFRARED-BASED IMPLICATIONS FOR THE DUST ATTENUATION AND STAR FORMATION OF TYPICAL LY α EMITTERS^{*,**}

HARUKA KUSAKABE^{1,*}, KAZUHIRO SHIMASAKU^{1,2}, KIMIHIKO NAKAJIMA³, AND MASAMI OUCHI^{4,5}

Accepted to ApJL (January 31st, 2015)

ABSTRACT

By stacking publicly available deep Spitzer/MIPS 24 μ m and Herschel/PACS images for 213 $z \simeq 2.18$ Ly α Emitters (LAEs) in GOODS-South, we obtain a strong upper limit to the IR luminosity of typical LAEs and discuss their attenuation curve for the first time. The 3σ upper limit $L_{\text{TIR}}^{3\sigma} = 1.1 \times 10^{10} L_{\odot}$, determined from the MIPS data providing the lowest limit, gives $\text{IRX} \equiv L_{\text{TIR}}/L_{\text{UV}} \leq 2.2$. Here we assume that the local calibration between the 8 μ m emission and the dust SED shape and metallicity applies at high redshifts and that our LAEs have low metallicities as suggested by previous studies. The inferred escape fractions of Ly α , 16–37%, and UV continuum, $\geq 44\%$, are higher than the cosmic averages at the same epoch. The SMC attenuation curve is consistent with the IRX and the UV slope $\beta = -1.4_{-0.2}^{+0.2}$ of our stacked LAE, while the Meurer’s relation (Calzetti curve) predicts a 3.8 times higher IRX; we also discuss the validity of PACS-based $L_{\text{TIR}}^{3\sigma}$ allowing the Meurer’s relation. SED fitting using the Calzetti curve also gives a ~ 10 times higher SFR than from the $L_{\text{TIR}}^{3\sigma}$ and L_{UV} . With $M_{\star} = 6.3_{-2.0}^{+0.8} \times 10^8 M_{\odot}$, our LAEs lie on a lower-mass extrapolation of the star formation main sequence at $z \sim 2$, suggesting that the majority of $z \sim 2$ LAEs are mildly star forming with relatively old ages of ~ 200 Myr. The faint $L_{\text{TIR}}^{3\sigma}$ implies that LAEs contribute little to the faint ($\gtrsim 100 \mu\text{Jy}$) submm number counts by ALMA.

1. INTRODUCTION

The IR luminosity of galaxies combined with the FUV luminosity provides a reliable measure of dust attenuation which is key to obtaining stellar population parameters such as star formation rate and stellar mass. However, at high redshift, because of the limited sensitivities of existing IR telescopes, luminosities have been measured only for relatively luminous galaxies ($L_{\text{TIR}} \gtrsim 10^{11} L_{\odot}$ at $z \gtrsim 2$, see, e.g., Elbaz et al. (2011); Magnelli et al. (2013)) except for a small number of less luminous, lensed galaxies (e.g., Sklias et al. 2014) and for stacked objects (e.g., Reddy et al. 2012). Considering the hierarchical nature of galaxy evolution, we also need to study faint galaxies.

Ly α emitters (LAEs) are suitable targets for studies of dust emission of faint galaxies because they typically have low ($\lesssim 10^9 M_{\odot}$) stellar masses (e.g., Guaita et al. 2011; Ono et al. 2010; Nakajima et al. 2012). How-

ever, previous studies have failed to individually detect dust emission from LAEs except for rare objects with (U)LIRG-like luminosities (Pentericci et al. 2010; Oteo et al. 2012). Wardlow et al. (2014) have stacked Herschel/SPIRE 250–500 μ m and LABOCA 870 μ m images of typical LAEs at $z \gtrsim 2.8$ to obtain 3σ upper limits of $L_{\text{TIR}} \sim 2\text{--}3 \times 10^{11} L_{\odot}$, but they have not discussed the amount of dust attenuation. Although, usually, SED fitting has thus been used to derive A_{1600} for LAEs, A_{1600} values from SED fitting are sensitively dependent on the attenuation curve assumed. All of the previous studies of LAEs have assumed the Calzetti curve (Calzetti et al. 2000) and obtained a relatively wide range of $A_{1600} \lesssim 3$ magnitude (see Table 2 of Vargas et al. (2014)). However, recent observations (e.g., Reddy et al. 2006; Nordon et al. 2013) have found that some high-redshift galaxies favor the Small Magellanic Cloud (SMC) curve (Pettini et al. 1998), which may question the use of the Calzetti curve for LAEs.

In this letter, we use a large sample of $z \simeq 2.18$ LAEs to obtain a strong upper limit to L_{TIR} using a stacking analysis of deep FIR data in GOODS South. After deriving the A_{1600} and total SFR, we discuss their attenuation curve and the mode of star formation. Also calculated are the submm flux density and the Ly α and UV escape fractions. We adopt a cosmology with $\Omega_{\Lambda} = 0.7$, $\Omega_m = 0.3$, and $H_0 = 70 \text{ km s}^{-1} \text{ Mpc}^{-1}$ and a Salpeter IMF.

2. DATA AND SAMPLE SELECTION

We select LAEs at $z = 2.18 \pm 0.04$ in the area covered by the deep Spitzer/MIPS 24 μ m data from the GOODS survey (Magnelli et al. 2011) and Herschel/PACS data from the PEP (Lutz et al. 2011) and GOODS-Herschel (Elbaz et al. 2011) surveys (Magnelli et al. 2013). The selection is performed in color-color space using Subaru/Suprime-Cam narrow-band NB387 data (Naka-

* kusakabe@astron.s.u-tokyo.ac.jp

¹ Department of Astronomy, Graduate School of Science, The University of Tokyo, 7-3-1 Hongo, Bunkyo-ku, Tokyo 113-0033, Japan

² Research Center for the Early Universe, The University of Tokyo, 7-3-1 Hongo, Bunkyo-ku, Tokyo 113-0033, Japan

³ Observatoire de Genève, Université de Genève, 51 Ch. des Maillettes, 1290 Versoix, Switzerland

⁴ Institute for Cosmic Ray Research, The University of Tokyo, 5-1-5 Kashiwanoha, Kashiwa, Chiba 277-8582, Japan

⁵ Kavli Institute for the Physics and Mathematics of the Universe (Kavli IPMU, WPI), The University of Tokyo, 5-1-5 Kashiwanoha, Kashiwa, Chiba 277-8583, Japan

* Based in part on observations made with the Spitzer Space Telescope, which is operated by the Jet Propulsion Laboratory, California Institute of Technology, under a contract with NASA.

** Based in part on observations with Herschel, an ESA space observatory with science instruments provided by European-led Principal Investigator consortia and with important participation from NASA.

jima et al. 2012) combined with VLT/VIMOS U -band (Nonino et al. 2009) and MPG 2.2m telescope/WFI B -band data (Hildebrandt et al. 2006) in essentially the same manner as Nakajima et al. (2012). After removing a small number of interlopers with a spectroscopic redshift outside of the range probed by NB387 ($z = 2.14 - 2.22$) ($\sim 6\%$) and Galactic stars ($\sim 0.4\%$) using the GOODS-MUSIC (Santini et al. 2009), the MUSYC (Cardamone et al. 2010), GMASS (Kurk et al. 2013), and X-ray (Chandra 4Ms; Xue et al. 2011) catalogs and AGNs ($\sim 2\%$) detected in X-ray or radio (VLA 1.4-GHz source catalog; Miller et al. 2013), we obtain a large sample of 213 LAEs down to $NB387 = 26.4$ magnitude (5σ , $2''$ diameter aperture) with average $M_{UV} = -18.7$ magnitude and $\sigma = 0.6$ magnitude.

3. STACKING ANALYSIS

3.1. FIR wavelengths

Since none of the 213 LAEs has a counterpart in either the MIPS⁶ or PACS catalog (Magnelli et al. 2013) within $1''$ radius, we perform the stacking analysis at the position of the LAEs in the MIPS/ $24\mu\text{m}$, PACS/ $70\mu\text{m}$, $100\mu\text{m}$, and $160\mu\text{m}$ bands. For MIPS/ $24\mu\text{m}$, before stacking, we remove sources listed in the MIPS catalog with a similar method to Reddy et al. (2012) and subtract a large-scale residual background following the procedure given in Wuyts et al. (2008). For each band, $50'' \times 50''$ cut-out images are median stacked. We then perform aperture photometry at the center of each stacked image on a radius of $3''.0$, $3''.2$, $4''.5$, and $7''.4$ for MIPS/ $24\mu\text{m}$, PACS/ $70\mu\text{m}$, $100\mu\text{m}$, and $160\mu\text{m}$, respectively. No significant signal is detected in any of the four stacked images, where the sky noise for each band is estimated from 1000 realizations generated by bootstrap resampling of the 213 objects as done by Wardlow et al. (2014). Thus, we derive the 3σ upper limit of the total flux density for each band by multiplying the 3σ sky noise by an aperture correction factor of 2.87, 2.45, 1.96, and 1.92 for MIPS/ $24\mu\text{m}$, PACS/ $70\mu\text{m}$, $100\mu\text{m}$, and $160\mu\text{m}$, respectively. The resulting 3σ total flux densities are 1.4, 56, 81, and $234\mu\text{Jy}$, respectively.

We calculate the upper limit of the infrared ($3 - 1000\mu\text{m}$) luminosity, L_{TIR} , of the stacked LAE using the MIPS and PACS 3σ data separately, by scaling the dust SED templates of local galaxies binned over various properties provided by Ciesla et al. (2014). For the MIPS data, we scale the lowest-metallicity template to the $24\mu\text{m}$ limit to obtain $L_{\text{TIR}}^{3\sigma} = 1.1 \times 10^{10} L_{\odot}$. We adopt this template because it gives the highest (i.e., most conservative) $L_{\text{TIR}}^{3\sigma}$ among all. For the PACS data, we fit the templates to a combination of the three data points to obtain $L_{\text{TIR}}^{3\sigma} = 1.4 \times 10^{11} L_{\odot}$ as the most conservative limit. We adopt the MIPS-based $L_{\text{TIR}}^{3\sigma}$ as the upper limit of our LAEs and use it in the following section.

Below we discuss the possibility that this MIPS-based $L_{\text{TIR}}^{3\sigma}$ may be optimistic. The MIPS/ $24\mu\text{m}$ band measures $\simeq 8\mu\text{m}$ PAH emission at $z \simeq 2.18$ and there is a well-known trend that the relative contribution of PAH emission to L_{TIR} decreases with decreasing metallicity (Galliano 2011). The lowest-metallicity template has

been constructed from galaxies with $12 + \log \text{O}/\text{H} \simeq 8.2 - 8.4$, which is consistent with those of $z \sim 2 - 3$ LAEs; bright LAEs, $12 + \log \text{O}/\text{H} \simeq 8.0 - 8.8$ (Nakajima & Ouchi 2014), and faint LAEs, $12 + \log \text{O}/\text{H} \simeq 8.2 \pm 0.1$ (Nakajima et al. 2012). Indeed, this template has a relatively high IR8 ($=L_{8-1000\mu\text{m}}/L_8$) of 6.7, being close to those of $z \sim 2$ UV-selected galaxies, $\simeq 8 - 9$ (Reddy et al. 2012), and significantly higher than the typical value of $z < 2.5$ star-forming galaxies ($\text{IR8} = 4$; Elbaz et al. 2011), and of Chary & Elbaz (2001) templates at the L_8 of our sample ($\text{IR8} \sim 4$). Starburst galaxies with high IR surface densities can also have high IR8 (Elbaz et al. 2011). However, even with the PACS-based $L_{\text{TIR}}^{3\sigma}$, the IR surface density of our LAEs is lower than the threshold for the starburst regime, $\simeq 3 \times 10^{10} L_{\odot} \text{ kpc}^{-2}$, where $\text{IR8} \simeq 8$. A 1 kpc half-light radius is assumed here (see, e.g., Hagen et al. (2014)).

Thus, it appears to be unlikely that the MIPS-based $L_{\text{TIR}}^{3\sigma}$ is significantly underestimating the true value. Note that the PACS-based $L_{\text{TIR}}^{3\sigma}$ divided by the L_8 of the lowest-metallicity template scaled to the MIPS photometry, gives $\text{IR8} \sim 90$. However, we should keep in mind that the derivation of the MIPS-based $L_{\text{TIR}}^{3\sigma}$ is based on two important assumptions that the local calibration between the $8\mu\text{m}$ emission and the dust SED shape and metallicity applies at high redshifts and that our LAEs have indeed low metallicities as suggested by previous studies.

3.2. Optical to MIR wavelengths

Forty-four percent of our LAEs are within the coverage of deep HST images from the GOODS and CANDELS surveys. Among them, we use 52 objects with uncontaminated IRAC images to obtain an HST F606W-centered, median image-stacked SED from optical to MIR wavelengths, which we assume to represent the entire sample and use for SED fitting. The images used for stacking are: the WFI B (Hildebrandt et al. 2006), the HST/ACS F606W, F775W, F850LP (Giavalisco et al. 2004)⁷, the HST/WFC3 F125W, F140W, F160W (Brammer et al. 2012; Grogin et al. 2011; Koekemoer et al. 2011; Skelton et al. 2014), and the Spitzer/IRAC $3.6\mu\text{m}$, $4.5\mu\text{m}$, $5.8\mu\text{m}$, $8.0\mu\text{m}$ (Damen et al. 2011). In photometry, the aperture radius and the aperture correction for the B and IRAC images are determined following the procedure of Ono et al. (2010). The aperture radius for the ACS/WFC images is set to $0''.9$ with an aperture correction factor of 1.07 (Skelton et al. 2014). Table 1 shows the total flux densities of the stacked SED, where the errors are a quadratic sum of the photometric error and error in zero point.

4. RESULTS AND DISCUSSION

4.1. Infrared Luminosity and Star Formation Rate

The 3σ luminosity obtained in Section 3.1, $L_{\text{TIR}}^{3\sigma} = 1.1 \times 10^{10} L_{\odot}$, is 200 times lower than the ‘knee’ luminosity of the IR luminosity function at $z \sim 2$ (Magnelli et al. 2013), implying that the majority of $z \sim 2$ LAEs have very faint dust emission.

⁶ <http://irsa.ipac.caltech.edu/cgi-bin/Gator/nph-search?mission=irsa&submit=Select&projshort=SPITZER>

⁷ The F450W image is not used because it is contaminated by Ly α emission at $z \simeq 2.18$.

The 3σ upper limit of the dust obscured star formation rate (SFR) is calculated to be $SFR_{\text{IR}} \leq 1.8 M_{\odot} \text{yr}^{-1}$ using the formula devised by Kennicutt (1998).

The unobscured SFR derived from the ultraviolet luminosity of the stacked SED, $L_{\text{UV}} = 5.3^{+0.2}_{-0.2} \times 10^9 L_{\odot}$ ($= L_{\text{UV, typical}}$), using the formula devised by Kennicutt (1998), is $SFR_{\text{UV}} = 1.5^{+0.07}_{-0.07} M_{\odot} \text{yr}^{-1}$. Thus, the ratio of obscured to unobscured SFRs is $SFR_{\text{IR}} / SFR_{\text{UV}} \leq 1.2$. This constraint is comparable or stronger than those for $z > 2$ LAEs obtained by Wardlow et al. (2014), $SFR_{\text{IR}} / SFR_{\text{UV}} \leq 2-14$. The total SFR is $1.5 \leq SFR_{\text{tot, IR+UV}} M_{\odot} \text{yr}^{-1} \leq 3.3$.

4.2. IRX- β and attenuation Curves

The relation between the IR to UV luminosity ratio, $IRX \equiv L_{\text{TIR}} / L_{\text{UV}}$, and the slope of the UV continuum, β , is useful for constraining the attenuation curve of galaxies. Our stacked LAE has $\beta = -1.4^{+0.2}_{-0.2}$ and $IRX \leq 2.2$ using the MIPS/24 μm -based $L_{\text{TIR}}^{3\sigma}$. This IRX corresponds to $A_{1600} \leq 0.9$ magnitude with the conversion formula by Overzier et al. (2011). This low IRX is in accord with the tendency seen in brighter UV-selected galaxies that IRX decreases with decreasing bolometric luminosity (e.g., Reddy et al. 2012). As found in Figure 1, these IRX and β are inconsistent with the relation for local starburst galaxies (Meurer et al. 1999) (M99, almost the same as the Calzetti curve) while consistent with an updated M99 given in Takeuchi et al. (2012) and the SMC curve (Pettini et al. 1998)⁸. The original M99 gives a 3.8 times higher IRX at the observed β .

All three attenuation curves assume an intrinsic slope $\beta_{\text{int}} \gtrsim -2.2$, while our best-fit SED model spectrum has $\beta_{\text{int}} = -2.6$ and -2.4 with the M99 and SMC curves, respectively (see sec 4.3). Adopting these bluer β_{int} instead of $\gtrsim -2.2$ increases the inconsistency of the M99 in the IRX- β plot while the SMC curve is still consistent.

The $z \sim 2$ UV selected galaxies of Reddy et al. (2012) are distributed around the M99 except for those with very young ages. LAEs and young UV selected galaxies may have similar attenuation curves.

The PACS-based $L_{\text{TIR}}^{3\sigma}$ gives a high $IRX = 28$ falling well above the M99. Indeed, the M99 is allowed in the case of $IRX \geq 8.4$. This happens if the MIPS-based $L_{\text{TIR}}^{3\sigma}$ is a factor of ≥ 3.8 underestimate, i.e. the true IR8 is higher than 26. However, as discussed in Section 3.1, such a high IR8 appears to be unlikely in our LAEs.

4.3. SED Fitting

We perform SED fitting on the stacked SED given in Table 1 to derive stellar population parameters with the procedure given in Ono et al. (2010), in which nebular emission is taken into account. We assume constant star formation history following previous SED studies of LAEs and examine the cases of the Calzetti and SMC curves. Although a stacked SED is not necessarily a good representation of individual objects (Vargas et al. 2014), stacking is still useful for our faint objects to obtain an SED covering rest-frame $> 1 \mu\text{m}$ and to consistently compare it with the stacked FIR SED.

⁸ We shift the original relation of Meurer et al. (1999) defined by $L_{\text{FIR}}(40-120 \mu\text{m})$ to 0.28dex.

Table 2 summarizes the best-fit parameters and Figure 2 compares the best-fit SEDs with the observed one. As expected from the results on the IRX- β plot, the fit using the Calzetti curve gives a 2 magnitude higher A_{1600} and 10 times higher SFR than those calculated from the MIPS-based $L_{\text{TIR}}^{3\sigma}$, while the results with the SMC curve are roughly consistent. The SFR from the SED fit with the Calzetti curve is significantly larger than even the maximum $SFR_{\text{tot, IR+UV}} = 24 M_{\odot} \text{yr}^{-1}$ from the PACS-based $L_{\text{TIR}}^{3\sigma}$. Both curves give nearly the same stellar mass, because it is determined essentially from longer wavelengths ($\gtrsim 1 \mu\text{m}$). The Calzetti curve gives an age less than 10 Myr, which is much shorter than dynamical times of LAEs, $\sim 60-260$ Myr (Rhoads et al. 2014). We also note that the Calzetti curve gives too high an escape fraction of ionizing photons $f_{\text{esc}}^{\text{ion}}$ compared with observed values for LAEs, 10–30% (Nestor et al. 2013). These results suggest that the SMC curve is more appropriate than Calzetti for the majority of LAEs at $z \sim 2$. With the SMC curve, our stacked LAE has an relatively old age of 200 Myr.

Nakajima et al. (2012) have provided a stacked SED of $z \simeq 2.18$ LAEs in the Subaru/XMM-Newton Deep Field for which a less dust-sensitive SFR estimate from narrow-band $\text{H}\alpha$ imaging is available. SED fitting to this stacked data finds that the E(B-V) derived assuming the Calzetti curve gives an $SFR_{\text{UV, corr}} (\simeq 32 M_{\odot} \text{yr}^{-1})$ which is two times higher than the $\text{H}\alpha$ -based one ($SFR_{\text{H}\alpha, \text{corr}} \simeq 14 M_{\odot} \text{yr}^{-1}$), while adopting the SMC curve gives a consistent result ($SFR_{\text{UV, corr}} \simeq 5.7 M_{\odot} \text{yr}^{-1}$, $SFR_{\text{H}\alpha, \text{corr}} \simeq 6.9 M_{\odot} \text{yr}^{-1}$). Notice that $E(B-V)_{\text{gas}} = E(B-V)_{\star}$ is assumed for modest dust-correction of the $\text{H}\alpha$ luminosity. Thus we find here that the SMC curve is preferred.

4.4. Mode of Star Formation

A relatively tight correlation is seen between SFR and M_{\star} at every redshift (Speagle et al. 2014). Galaxies on this star formation main sequence (SFMS) are thought to form stars steadily, perhaps being in an equilibrium between gas consumption and accretion, while those above the SFMS are forming stars burstly.

As found in Figure 3, our LAEs lie on a lower-mass extrapolation of the SFMS⁹ defined by massive galaxies ($M_{\star} > 10^{10} M_{\odot}$; Daddi et al. 2007; Rodighiero et al. 2011). This suggests that the majority of $z \simeq 2.18$ LAEs are in the ‘normal’ star-formation mode and that the SFMS appears to continue down to below $M_{\star} = 10^9 M_{\odot}$. Note that adopting the Calzetti curve leads us to conclude that they are undergoing starburst. On the other hand, most of the extremely luminous, individually detected LAEs at $z \sim 2$ by Hagen et al. (2014) are burst-like galaxies. The individually detected LAEs by Vargas et al. (2014) also tend to be bursty. Both authors have used the Calzetti curve. One possibility is that the star formation modes of LAEs studied in these papers and our LAEs are different. The other is that some of their LAEs also have an SMC-like attenuation curve and hence their SFRs are predicted to shift towards the SFMS.

⁹ Figure 17 of the Daddi et al. (2007) suggests that the Calzetti curve applies to BzK galaxies.

4.5. Can LAEs be Candidates of Faint Submillimeter Galaxies ?

Recent deep ALMA observations have revealed an abundant population of faint (down to $\gtrsim 100 \mu\text{Jy}$ at $\lambda \simeq 1 \text{ mm}$) SMGs (Ono et al. 2014). Optical counterparts to them remain to be identified and LAEs are on a list of potential candidates (Ono et al. 2014). We find that galaxies with $L_{\text{TIR}}^{3\sigma}$ have relatively constant 1.2-mm flux densities of $\sim 10 \mu\text{Jy}$ over a wide redshift range of $z \gtrsim 1$ due to the so-called negative k correction. Therefore, typical LAEs are unlikely to be major counterparts to the faint SMGs unless they significantly evolve in L_{TIR} with redshift. This is not to rule out the possibility that rare, luminous ($L_{\text{UV}} \gtrsim 10 \times L_{\text{UV, typical}}$) LAEs are detectable with ALMA, although a luminous Ly α blob at $z \simeq 6.6$, Himiko, is undetected with ALMA at 1.2mm and its strong upper limit, $52 \mu\text{Jy}$ (Ouchi et al. 2013), is consistent with our value. Deep ALMA observations of luminous LAEs can also be useful, even with non detection, for discriminating between attenuation curves combined with β measurements.

4.6. Escape Fractions of Ly α and UV Continuum

The escape fractions of Ly α and UV continuum photons are robustly constrained from $L_{\text{TIR}}^{3\sigma}$. By stacking the 52 LAEs in the NB387 band, we obtain $L(\text{Ly}\alpha) = 5.9_{-0.6}^{+0.6} \times 10^{41} \text{ erg s}^{-1}$, which is converted into $\text{SFR}_{\text{Ly}\alpha} = 0.54_{-0.6}^{+0.6} \text{ M}_{\odot} \text{ yr}^{-1}$ (Brocklehurst 1971; Kennicutt 1998). Here we have assumed that the NB387 photometry recovers the total Ly α luminosity. Since the intrinsic Ly α luminosity can be calculated from the total SFR, the escape fraction of Ly α is constrained as:

$$16\% = \frac{\text{SFR}_{\text{Ly}\alpha}}{\text{SFR}_{\text{UV}} + \text{SFR}_{\text{IR}}^{3\sigma}} \leq f_{\text{esc}}^{\text{Ly}\alpha} \leq \frac{\text{SFR}_{\text{Ly}\alpha}}{\text{SFR}_{\text{UV}}} = 37\%. \quad (1)$$

This constraint on $f_{\text{esc}}^{\text{Ly}\alpha}$ is roughly consistent with that based on the H α luminosity (Nakajima et al. 2012) as well as the lower limits obtained by Wardlow et al. (2014) from FIR stacking. The escape fraction of UV continuum photons is constrained to be:

$$f_{\text{esc}}^{\text{UV}} = 10^{-0.4 \times A_{1600}} \geq 44\%. \quad (2)$$

These $f_{\text{esc}}^{\text{Ly}\alpha}$ and $f_{\text{esc}}^{\text{UV}}$ values are significantly higher than the cosmic averages at $z \sim 2$, $f_{\text{esc}}^{\text{Ly}\alpha} \simeq 2.8_{-0.4}^{+2.6}\%$ (Hayes et al. 2011) and $f_{\text{esc}}^{\text{UV}} \simeq 22_{-7}^{+12}\%$ (Burgarella et al. 2013), but comparable to those at $z \gtrsim 4$. A number of mechanisms (e.g., outflow and clumpy ISM distribution) have been proposed that make the escape of Ly α photons easy in LAEs. This study would suggest that for the majority of LAEs absolute low dust attenuation is an important factor.

We thank the anonymous referee for helpful comments and suggestions. We are grateful to Yoshiaki Ono for useful comments on SED fitting. We thank Giulia Rodighiero and Alex Hagen for kindly providing their data plotted in Figure 3. We acknowledge

Tamami I. Mori, Tsutomu Takeuchi, Eric Gawiser, Mark Hammonds, Ronin Wu, Ryota Kawamata, Takuya Hashimoto, Ryousuke Goto, Shingo Shinogi, and Akisa Ono for useful discussions and comments on this letter. This work is based on observations taken by the CANDELS Multi-Cycle Treasury Program with the NASA/ESA HST, which is operated by the Association of Universities for Research in Astronomy, Inc., under NASA contract NAS5-26555 and observations taken by the 3D-HST Treasury Program (GO 12177 and 12328) with the NASA/ESA HST, which is operated by the Association of Universities for Research in Astronomy, Inc., under NASA contract NAS5-26555. This work is also based on the GOODS-MUSIC catalog.

Facilities: Subaru (Suprime-Cam), Spitzer (IRAC, MIPS), Herschel (PACS), HST (ACS, WFC3), VLT (VIMOS), MPG 2.2m telescope (WFI)

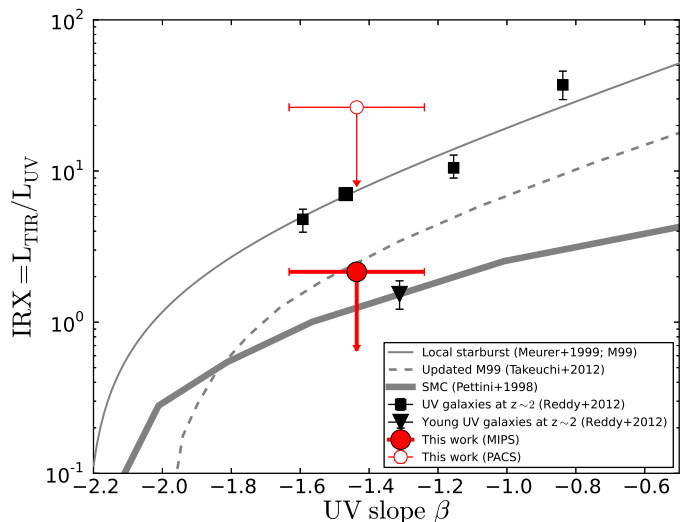


FIG. 1.— The $L_{\text{TIR}}/L_{\text{UV}}$ ratio, IRX, plotted against the UV slope, β . The red filled and open circles indicate our stacked LAE from the MIPS and PACS data, respectively. The black squares are for the stacking results for UV-selected galaxies binned according to various properties obtained by Reddy et al. (2012) (largest symbol corresponding to the entire sample) and the black triangle for the stacking result for young galaxies (Reddy et al. 2012). Three attenuation curves are overplotted: the local starburst relation (thin solid line; Meurer et al. (1999, M99)); an updated M99 (dashed line; Takeuchi et al. (2012)); the SMC curve (thick solid line; Pettini et al. (1998)).

TABLE 1
BROADBAND PHOTOMETRY OF THE STACKED LAE FROM OPTICAL TO MIR

B	$F606W$	$F775W$	$F850LP$	$F125W$	$F140W$	$F160W$	[3.6]	[4.5]	[5.8]	[8.0]
0.092 (0.007)	0.11 (0.005)	0.12 (0.008)	0.15 (0.01)	0.21 (0.01)	0.25 (0.03)	0.26 (0.02)	0.24 (0.05)	0.18 (0.05)	0.13 (0.2)	0.09 (0.1)

NOTE. — All flux densities are total flux densities in μJy , with 1σ errors shown in parentheses.

TABLE 2
RESULTS OF SED FITTING

attenuation curve	M_* [$10^8 M_\odot$]	$E(B-V)_*$ [A_{1600}] [mag]	Age [Myr]	SFR [$M_\odot \text{yr}^{-1}$]	$f_{\text{esc}}^{\text{ion}}$	χ_r^2	$SFR_{\text{UV,corr}}$ [$M_\odot \text{yr}^{-1}$]
Calzetti	$3.7^{+0.1}_{-0.1}$	$0.3^{+0.00}_{-0.00}$ [$3.0^{+0.0}_{-0.0}$]	$8.7^{+0.8}_{-1.1}$	43^{+4}_{-2}	$0.9^{+0.0}_{-0.0}$	1.02	25^{+1}_{-1}
SMC	$6.3^{+0.8}_{-2.0}$	$0.10^{+0.02}_{-0.01}$ [$1.2^{+0.2}_{-0.1}$]	200^{+50}_{-100}	$3.7^{+1.2}_{-0.4}$	$0.4^{+0.3}_{-0.3}$	1.22	$4.9^{+1.7}_{-0.3}$

NOTE. — Metallicity and redshift are fixed to $0.2Z_\odot$ and 2.18, respectively. The degree of freedom is 7. SFR is not a free parameter in the fit but calculated from M_* and age. $SFR_{\text{UV,corr}}$ is derived from the dust-corrected UV luminosity using A_{1600} .

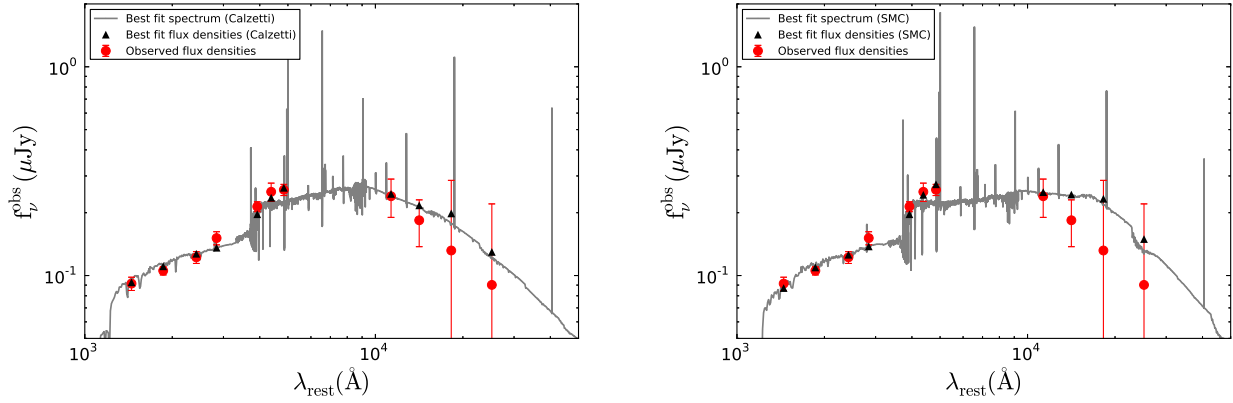


FIG. 2.— Results of SED fitting with the Calzetti curve (left) and the SMC curve (right). For each panel, the red filled circles show the observed flux densities, the gray lines the best-fit model spectrum, and the black filled triangles the flux densities calculated from the best-fit spectrum. The two attenuation curves fit the data well.

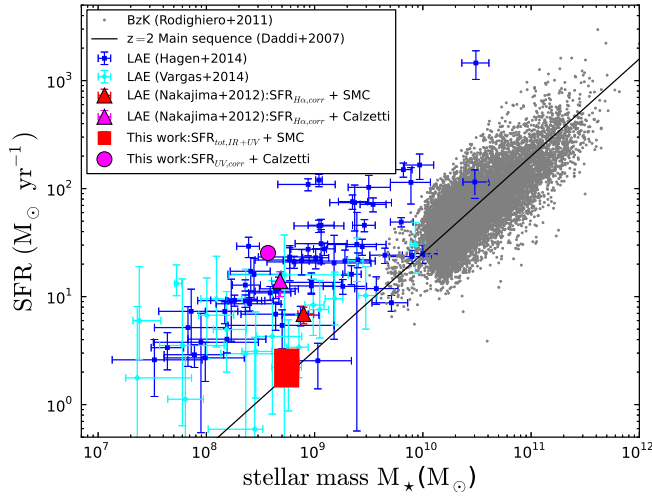


FIG. 3.— SFR_{tot} plotted against M_{\star} . The red rectangular region represents our stacked LAE with $M_{\star} = 6.3^{+0.8}_{-2.6} M_{\odot}$ from the SMC curve and $SFR_{\text{tot,IR+UV}} = 1.5\text{--}3.3 M_{\odot} \text{ yr}^{-1}$, while the magenta filled circle corresponds to the result from the SED fitting with the Calzetti curve ($SFR = SFR_{\text{UV,corr}}$). The red and magenta triangles represent LAE from Nakajima et al. (2012), calculated from $SFR_{H\alpha, \text{corr}}$ using the A_{1600} obtained by the SED fitting with the SMC curve and the Calzetti curve, respectively. The black line shows the star formation main sequence at $z = 2$ (Daddi et al. 2007) and the gray dots represent BzK galaxies (Rodighiero et al. 2011). The blue and cyan dots are for LAEs given in Hagen et al. (2014) and Vargas et al. (2014), respectively; for both samples the Calzetti curve has been used to derive A_{1600} .

REFERENCES

- Brammer, G. B., van Dokkum, P. G., Franx, M., et al. 2012, *The Astrophysical Journal Supplement Series*, 200, 13
- Brocklehurst, M. 1971, *MNRAS*, 153, 471
- Burgarella, D., Buat, V., Gruppioni, C., et al. 2013, *A&A*, 554, 70
- Calzetti, D., Armus, L., Bohkin, R., et al. 2000, *ApJ*, 533, 682
- Cardamone, C. N., van Dokkum, P. G., Urry, C. M., et al. 2010, *The Astrophysical Journal Supplement Series*, 189, 270
- Chary, R., & Elbaz, D. 2001, *ApJ*, 556, 562
- Ciesla, L., Boquien, M., Boselli, A., et al. 2014, *A&A*, 565, 128
- Daddi, E., Dickinson, M., Morrison, G., et al. 2007, *ApJ*, 670, 156
- Damen, M., Labbé, I., van Dokkum, P. G., et al. 2011, *The Astrophysical Journal*, 727, 1
- Elbaz, D., Dickinson, M., Hwang, H. S., et al. 2011, *A&A*, 533, 119
- Galliano, F. 2011, *EAS Publications Series*, 46, 43
- Giavalisco, M., Ferguson, H. C., Koekemoer, A. M., et al. 2004, *ApJ*, 600, 93
- Grogin, N. a., Kocevski, D. D., Faber, S. M., et al. 2011, *The Astrophysical Journal Supplement Series*, 197, 35
- Guaita, L., Acquaviva, V., Padilla, N., et al. 2011, *The Astrophysical Journal*, 733, 114
- Hagen, A., Ciardullo, R., Gronwall, C., et al. 2014, *The Astrophysical Journal*, 786, 59
- Hayes, M., Schaerer, D., Östlin, G., et al. 2011, *The Astrophysical Journal*, 730, 8
- Hildebrandt, H., Erben, T., Dietrich, J., et al. 2006, *A&A*, 452, 1121
- Kennicutt, R. C. 1998, *Annual Review of Astronomy and Astrophysics*, 36, 189
- Koekemoer, A. M., Faber, S. M., Ferguson, H. C., et al. 2011, *The Astrophysical Journal Supplement Series*, 197, 36
- Kurk, J., Cimatti, A., Daddi, E., et al. 2013, *A&A*, 549, 63
- Lutz, D., Poglitsch, A., Altieri, B., et al. 2011, *A&A*, 532, 90
- Magnelli, B., Elbaz, D., Chary, R. R., et al. 2011, *A&A*, 528, 35
- Magnelli, B., Popesso, P., Berta, S., et al. 2013, *A&A*, 553, 132
- Meurer, G. R., Heckman, T., & Calzetti, D. 1999, *ApJ*, 521, 64
- Miller, N. a., Bonzini, M., Fomalont, E. B., et al. 2013, *The Astrophysical Journal Supplement Series*, 205, 13
- Nakajima, K., & Ouchi, M. 2014, *Monthly Notices of the Royal Astronomical Society*, 442, 900
- Nakajima, K., Ouchi, M., Shimasaku, K., et al. 2012, *The Astrophysical Journal*, 745, 12
- Nestor, D. B., Shapley, A. E., Kornei, K. a., Steidel, C. C., & Siana, B. 2013, *The Astrophysical Journal*, 765, 47
- Nonino, M., Dickinson, M., Rosati, P., et al. 2009, *The Astrophysical Journal Supplement Series*, 183, 244
- Nordon, R., Lutz, D., Saintonge, a., et al. 2013, *The Astrophysical Journal*, 762, 125
- Ono, Y., Ouchi, M., Kurono, Y., & Momose, R. 2014, *The Astrophysical Journal*, 795, 5
- Ono, Y., Shimasaku, K., Dunlop, J., et al. 2010, *The Astrophysical Journal*, 724, 1524
- Oteo, I., Bongiovanni, A., Cepa, J., et al. 2012, *A&A*, 541, A65
- Ouchi, M., Ellis, R., Ono, Y., et al. 2013, *The Astrophysical Journal*, 778, 102
- Overzier, R. a., Heckman, T. M., Wang, J., et al. 2011, *The Astrophysical Journal*, 726, L7
- Pentericci, L., Grazian, A., Scarlata, C., et al. 2010, *A&A*, 514, A64
- Pettini, M., Ellogg, M. E. K., Teidel, C. H. C. S., & Delberger, K. U. R. T. L. A. 1998, *ApJ*, 508, 539
- Reddy, N., Dickinson, M., Elbaz, D., et al. 2012, *The Astrophysical Journal*, 744, 154
- Reddy, N. A., Steidel, C. C., Fadda, D., et al. 2006, *ApJ*, 644, 792
- Rhoads, J. E., Malhotra, S., Richardson, M. L. a., et al. 2014, *The Astrophysical Journal*, 780, 20
- Rodighiero, G., Daddi, E., Baronchelli, I., et al. 2011, *The Astrophysical Journal*, 739, L40
- Santini, P., Fontana, A., Grazian, A., et al. 2009, *A&A*, 504, 751
- Skelton, R. E., Whitaker, K. E., Momcheva, I. G., Brammer, G. B., & Dokkum, P. G. 2014, *ApJ*, 214, 24
- Sklias, P., Zamojski, M., Schaerer, D., et al. 2014, *A&A*, 561, A149
- Speagle, J. S., Steinhart, C. L., Capak, P. L., & Silverman, J. D. 2014, *The Astrophysical Journal Supplement Series*, 214, 15
- Takeuchi, T. T., Yuan, F.-T., Ikeyama, A., Murata, K. L., & Inoue, A. K. 2012, *The Astrophysical Journal*, 755, 144
- Vargas, C. J., Bish, H., Acquaviva, V., et al. 2014, *The Astrophysical Journal*, 783, 26
- Wardlow, J. L., Malhotra, S., Zheng, Z., et al. 2014, *The Astrophysical Journal*, 787, 9
- Wuyts, S., Labbe, I., Fo, N. M., et al. 2008, *ApJ*, 682, 985
- Xue, Y. Q., Luo, B., Brandt, W. N., et al. 2011, *The Astrophysical Journal Supplement Series*, 195, 10